FUNDAMENTALS & APPLICATIONS

CHEMELECTROCHEM

ANALYSIS & CATALYSIS, BIO & NANO, ENERGY & MORE

Accepted Article

Title: Electrocatalytical activity of ionic liquid-derived porous carbon materials for oxygen reduction reaction

Authors: Nikola Zdolsek, Aleksandra Dimitrijevic, Magdalena Bendova, Jugolav Krstic, Raquel P Rocha, Jose L Figueiredo, Danica Bajuk-Bogdanovic, Tatjana Trtic-Petrovic, and Biljana Sljukic Paunkovic

To be cited as: *ChemElectroChem* 10.1002/celc.201701369

Link to VoR: http://dx.doi.org/10.1002/celc.201701369

A Journal of

ChemPubSoc Europe

WILEY-VCH

www.chemelectrochem.org

ARTICLE WILEY-VCH

Electrocatalytical activity of ionic liquid-derived porous carbon materials for oxygen reduction reaction

Nikola Zdolšek,[b] Aleksandra Dimitrijević,[b] Magdalena Bendova,[c] Jugoslav Krstić,[d] Raquel P. Rocha,[e] José L. Figueiredo,[e] Danica Bajuk-Bogdanović,[a] TatjanaTrtić-Petrović,[b] and Biljana Šljukić*[a]

Abstract: Carbon materials, prepared by different methods using ionic liquid, are compared as electrocatalysts for oxygen reduction reaction (ORR). Materials were synthesized by hydrothermal carbonization of glucose and by the same method in the presence of 1-butyl-3-methylimidazolium methanesulfonate [bmim][$MeSO_3$] as additive. Other two carbon materials were prepared by ionic-liquid based methods: ionothermal carbonization of glucose using [bmim][$MeSO_3$] as recyclable medium for carbonization reaction and by direct carbonization of ionic liquid, one step method using [bmim][$MeSO_3$] as precursor for N- and S-doped porous carbon (Carb-IL).Characterization results showed possibility of morphology and porosity control using [bmim][$MeSO_3$]. All materials were subsequently tested for ORR in alkaline media. Carb-IL showed the enhanced and stable electrocatalytic ORR activity, even in the presence of methanol, ethanol and borohydride, opening possibility for its application in fuel cells.

1. Introduction

The cathodic oxygen reduction reaction (ORR) is an important process in energy conversion systems such as fuel cells and lithium-air batteries, gas sensors and in the electrosynthesis of hydrogen peroxide (H_2O_2).[1] Nowadays, the ORR is one of the most important challenges and widely studied reaction in electrochemistry. The ORR in aqueous solution can proceed by two pathways.[2] One is a direct four-electron pathway, in which O_2 is reduced directly to water, without generation of intermediates such as H_2O_2. The other is two-step two-electron pathway, in which H_2O_2 is formed as an intermediate. The four-electron pathway is required for high energy conversion efficiency of fuel cells. Still, the slow ORR kinetics represents limiting factor for efficient energy conversion in fuel cells. In order to improve ORR kinetics, and therefore to improve the fuel cell efficiency, different cathodic electrocatalysts have been developed.[3]

Recently, rapid growth of nanostructured carbon materials such as carbon nanotubes, porous carbon and graphene, have attracted interests for these materials as metal-free catalysts for ORR.[4] These carbon materials exhibit high thermal and chemical stability, high surface area, electrical conductivity, methanol tolerance and low cost. Physico-chemical properties as well as electrocatalytical activity can be improved by doping carbon materials with other, foreign, elements. Nitrogen-doped carbon materials have been extensively studied as the catalysts for the ORR.[5] Doping carbon materials with other dopants such as boron, phosphorus, sulphur, selenium and iodine and their use in ORR has also been reported.[6] Binary- and ternary-doped carbons exhibited higher electrocatalytic activity for ORR, compared with a single atom-doped carbon.[7] Carbonisation of C-reach precursors at high temperatures is the most common method for production of carbon materials. Hydrothermal carbonization (HTC) of raw biomass (glucose, sucrose, fructose), under mild temperatures (180-200°C) and self-generated pressure, is a commonly used method for the preparation of porous carbons.[8] The introduction of heteroatom in HTC of biomass has been achieved in the presence of heteroatom dopant, but doped carbons can also be produced in direct carbonization of heteroatom-containing precursor in an inert atmosphere at high temperature.[9] The main drawback of this method is the limited source of precursors and complicated procedure in case of carbon materials with task specific properties, such as desirable specific surface area, morphology and surface chemistry. This drawback can be solved by new strategy, using ionic liquids (ILs) for carbon materials synthesis.

In the past few years, ILs found application in the synthesis of new materials, especially carbon-based materials *via* ionothermal carbonization (ITC) of biomass.[10] Unique physicochemical properties make ILs an advanced green reaction medium for ITC; therefore ITC presents more advantages than HTC. Due to low vapour pressure and low volatility, conversion of biomass occurs at ambient pressure in stable reaction environment without significant self-generated pressures.[11] The structural diversity of ILs cation-anion combinations offers the possibility for morphology and porosity control. Hence, ILs can be used as structural directing agents and templates for porosity generation without additional templates such as silica templates in hydrothermal carbonization.[12] ILs act as an effective catalyst for carbohydrate dehydration resulting in enhanced yields for ionothermal

[a] Dr.D.Bajuk-Bogdanović; Dr.B.Šljukić
Faculty of Physical Chemistry, University of Belgrade
Studentskitrg 12-16, 11158, Belgrade (Serbia)
E-mail: biljka@ffh.bg.ac.rs
[b] N.Zdolšek; A.Dimitrijević; Dr.T.Trtić-Petrović
Laboratory of Physics
Vinča Institute of nuclear sciences, University of Belgrade
P.O. Box 522, 11001, Belgrade (Serbia)
[c] Dr.M. Bendova
E. Hála Laboratory of Separation Processes,
Institute of Chemical Process Fundamentals of the CAS, v. v. i.,
Rozvojová 135/1, Prague (Czech Republic)
[d] Dr.J.Krstić
Department of Catalysis and Chemical Engineering,
Institute of Chemistry, Technology and Metallurgy,University of Belgrade
Njegoševa 12, Belgrade(Serbia)
[e] R.P.Rocha, Dr.J.L.Figueiredo
Laboratory of Catalysis and Materials – Associate Laboratory LSRE-LCM,
Faculdade de Engenharia, Universidade do Porto
R. Dr. Roberto Frias, 4200–465, Porto (Portugal)

Supporting information for this article is given via a link at the end of the document.

carbons (80%), compared to hydrothermal carbons (40%).[13] Also important from green chemistry aspects, is that ILs can be recovered at the end of each carbonization reaction and reused.[11,14] Finally, ILs can be used as fluid precursors for functional carbons *via* direct carbonization of ILs.[15] This method represents a very simple, one step, synthesis route for carbon materials since ILs act as a self-porogen and dopant precursors in the absence of additional solvents. Due to the possibility of design and synthesis of vast number of different IL, ILs as precursors for carbon materials with various dopants create a new platform for easy investigation of dopants influence on material's catalytical activity.

Since the synthesis and functionalization of carbon materials based on ILs is still at an early stage, as well application of ionic liquid-derived carbon materials, the purpose of this work was to compare and characterize carbon materials for the ORR obtained by four different methods: hydrothermal carbonization of glucose, IL-enhanced hydrothermal carbonization, ionothermal carbonization and direct carbonization of IL. 1-butyl-3-methylimidazolium methanesulfonate [bmim][$MeSO_3$] was used as an ionothermal medium for the conversion of glucose precursor into porous carbon and as precursor for sulphur- and nitrogen-doped porous carbon. To the best of our knowledge, such carbon materials have not yet been compared for ORR and [bmim][$MeSO_3$] has not been used as additive, medium and single carbon precursor for one step synthesis of carbon materials (with specific morphology, textural properties and surface chemistry) without additional substances, templates nor nanocasting methods.

2. Results and Discussion

2.1 Yields of carbon materials and recovery of studied ionic liquid

Three carbon materials (Carb-IL, ITC and HTC+IL) were synthesised based on ionic liquid through different novel synthesis approaches: direct carbonization of IL, ionothermal carbonization and IL-enhanced hydrothermal carbonization. Carbon material synthetized by conventional hydrothermal carbonization of glucose (HTC) was prepared for comparison purposes. The product yield of the ITC@200 was 46% and higher than the corresponding HTC@200 and HTC+IL@200 (31% and 29%, respectively). This highest carbon yield for ITC@200 could be attributed to the catalytic activity of IL for carbohydrate dehydration and 5-hydroxymethylfurfural (HMF) production and to enhanced conditions for the dehydration, polymerization and carbonization reactions that form the carbonaceous network.[13] After thermal treatment at 900 °C, the yield was about 50% lower, the yield of carbon obtained by direct carbonization of IL (Carb-IL) was 8.5 %.

High thermally stable [bmim][$MeSO_3$] with sulphur and nitrogen atoms in the structure and with possibility to dissolve D(+)glucose was chosen for carbon materials synthesis. HML method, used for determination of melting temperature, is based on the Heat-Leak-Modulus developed by Quirion et al. and this method allows a simple thermal analysis of materials.[16] The information provided by the HLM method is essentially equivalent to that obtained from differential scanning calorimetry (DSC) measurement. While being more robust than DSC, it provides a good reproducibility of the measured temperatures of melting and is thus suitable for a quick screening of the phase transitions in the studied materials. For instance, it has been successfully applied in a study of the binary system of ethylammonium nitrate with acetonitrile.[17] In this work, five independent measurements of the melting temperature were carried out in a preliminary screening. The melting temperature was then found to be of 74°C. The repeatability of the measurements was determined as 0.5°C non-statistically by means of marginal analysis, a method based on mathematical Gnostic.[18] Thermogravimetric analysis (TGA) of [bmim][$MeSO_3$] confirmed high thermal stability; decomposition started at 262°C so at temperature higher than 400°C, [bmim][$MeSO_3$] was completely decomposed with relative weight loss of about 90%.[19] The mentioned high thermal stability of [bmim][$MeSO_3$] is also important from recycling aspect of ionic liquid after ionothermal carbonization. The recovery of the IL used in ITC was 98%. Comparison of FT-IR and Raman spectra of pure and recovered IL shows no differences between these samples (Figure S1 in the ESI) and these data indicate that IL was successfully recovered. This result suggests conversion of biomass through ionothermal carbonization as a green reusable synthesis method for porous carbon materials.

2.2 Characterisation of the carbon materials

Figure 1 shows SEM micrographs of the obtained carbon materials. It is evident that the morphology of the obtained carbon materials depends on the synthesis method as well as on the precursors.

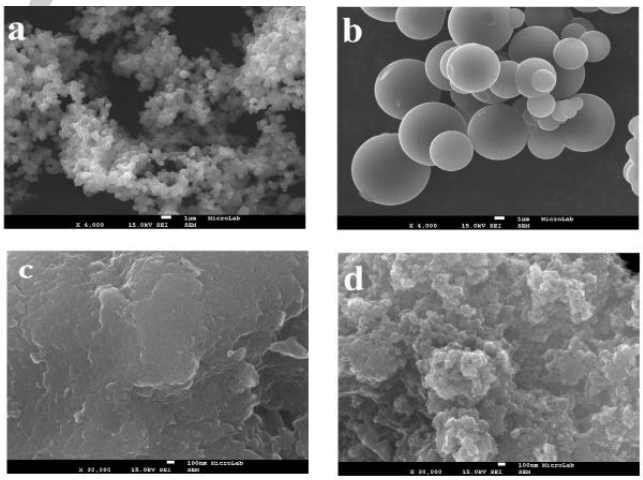

Figure 1. SEM micrographs of a) HTC; b) HTC+IL; c) ITC and d) Carb-IL.

HTC is made up of spherical particles with diameter <1μm, randomly dispersed inside an interconnected matrix, which is the typical morphology of carbons prepared by hydrothermal carbonization.[20] HTC+IL consists of carbon spheres with diameter of 5 – 10 μm and smooth surfaces. In this case, the

ionic liquid may act as a structure forming agent. On the other hand, morphologies of ITC and Carb–IL are different compared to hydrothermal carbons. In ionothermal carbonization, morphology and porosity of final materials are the result of interaction of formed carbonaceous network and the ionic liquid.[13] Namely, IL acts as structure forming agent and template and obtained morphology could be attributed to the structure of used IL and interaction between IL and carbon precursor during ionothermal carbonization. Morphology with microparticles and lumps of different sizes was obtained for ITC. SEM micrograph of Carb–IL indicates sponge-like carbonaceous nanomorphology, which depend only on IL structure, since [bmim][$MeSO_3$] was used as precursor for porous carbon.

Furthermore, nitrogen adsorption analysis showed differences in specific surface area (S_{BET}) values of the four materials. The values of S_{BET} were 147.0, 195.0, 278.4 and 509.0 m^2 g^{-1} for HTC+IL, ITC, Carb-IL and HTC, respectively. The lowest S_{BET} values for HTC+IL and ITC was expected since symmetry and size of ionic liquids anion play dominant role in the development of surface area, with large anions giving carbon materials of high specific surface area.[21] Methanesulfonate is a small anion leading to carbon material of relatively low S_{BET} value. Lower S_{BET} value (160 m^2 g^{-1}) was obtained for carbon material synthesised by ionothermal carbonization of glucose using 1-butyl-3-methyl imidazolium tetrachloroferrate in which anion is smaller compared to methanesulfonate.[13] Reasonably high surface area was obtained for Carb-IL, though lower than that of HTC. Like on the morphology of Carb-IL, IL structure, both cation and anion influence the final surface area of carbon material prepared by direct carbonization of IL.[15a] It is known that aromatic-amines-based cations, such as imidazolium ring in [bmim][$MeSO_3$], lead to carbon materials of acceptably high surface area. Contrary, cations with unsaturated moiety or C=C bonds lead to carbon materials of lower surface area. Furthermore, anion of IL also takes part in specific surface area formation as porogens or template to generate large amounts of pores. Thus, carbonaceous materials derived from bulky anions feature high surface areas.[22] Synergic effects of cation and anion of [bmim][$MeSO_3$] lead to Carb-IL of specific surface area of 278.4 m^2 g^{-1}. All these results demonstrate the control of morphology and specific surface area of obtained carbon materials using [bmim][$MeSO_3$] either as additive, medium or a single carbon precursor without additional templates and nanocasting methods.

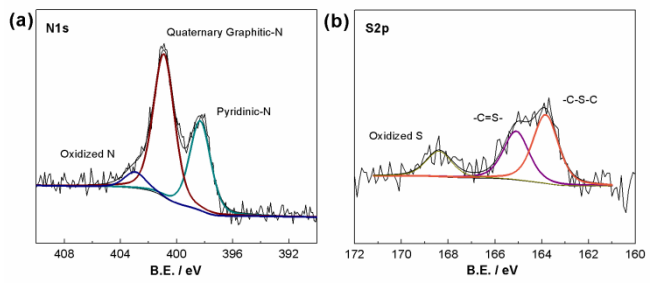

Figure 2.(a) N1s XPS spectrum and (b) S2p spectrum recorded from Carb-IL sample corresponding fittings.

Table 1. Surface composition determined by XPS.

Sample	Surface composition (wt. %)			
	C	N	O	S
HTC	82.8	n.d	17.2	n.d
HTC+IL	90.4	n.d	9.9	n.d
ITC	90.1	n.d	9.6	n.d
Carb-IL	81.4	3.2	14.9	0.5

n.d-not detected

Surface composition of the carbon materials was determined by XPS analysis (Table 1). All samples are characterized by a carbon/oxygen matrix, except the Carb-IL sample that revealed the presence of nitrogen and sulphur in its composition as well (3.2 % of N and 0.5 % of S). Independently of the synthesis route, carbon is the most abundant component (always higher than 80 %): samples HTC and Carb-IL present 82.8 and 81.4 % of carbon and 17.2 and 14.9 % of oxygen, respectively, while samples ITC and HTC+IL revealed around 10 % of oxygen.

The presence of N and S in Carb-IL sample is directly related to the presence of functional groups of the IL; upon polymerization at high temperatures, nitrogen-doped graphitic microdomains are formed.[23] The polymerization during the decomposition is enhanced by cations that must be nitrogen containing, such as imidazolium, and by a reactive anion functionality, typically a cyano group.[10,13,23,24] In this study, the methanesulfonate anion was shown to also provide enhanced conditions for formation of a N-, S-rich carbonaceous network. Upon thermal degradation of ILs, functionalities energetically prefer to bend rather than to being terminal, therefore, edge structures are not usually observed. Deconvolution of the N1s spectrum of the Carb-IL sample (Figure 2a) revealed the presence of nitrogen predominantly bonded as pyridinic-N (at 398.3 eV) and quaternary graphitic nitrogen (at 400.9 eV) as structural nitrogen incorporated into graphitic microdomains (36 and 57 % of the total nitrogen content, respectively) and lower amounts of oxidised nitrogen-species (7 % at 403.0 eV), in agreement with previous reports.[23,24a] Regarding the S2p spectrum deconvolution, some assumptions were taken into account: sulphur can be incorporated into a carbon surface as elemental sulphur (S8 rings),[25] but seldom occupying the periphery of graphitic layers.[26] The possible configurations of sulphur incorporated into the graphitic carbon framework depend on the synthesis conditions, and, therefore, some groups are favoured while others are eliminated. At moderate/low temperatures (<400 ºC), sulfonic groups, thiols and disulphide are formed, but with the increase of the carbonization temperature the formation of thiophene species is promoted, as result of the transformation of sulphides, thiols and sulphones. The Sp2 spectrum of Carb-IL sample (Figure 2b) presents a well-defined peak at 163.8 eV,

characteristic binding energy of the thiophene-like group representing 48% of the total sulphur content. The presence of ─C=S─ is detected (34 %) at 165.1 eV, as well as oxidised S species (C-SO_x) at 168.4 eV.[27] The results clearly reveal that [bmim][$MeSO_3$] fulfils the structural requirements to produce a N-, S- codoped carbon material.

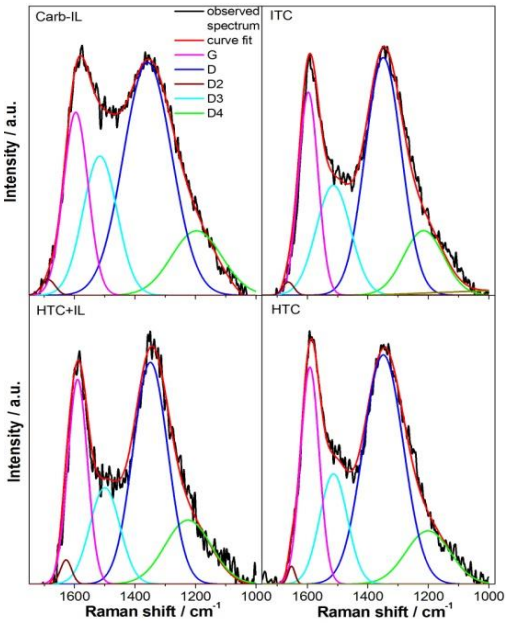

Figure 3. Deconvoluted Raman spectrum of Carb–IL; ITC; HTC+IL and HTC.

Figure 3 represents Raman spectra of the obtained materials deconvoluted using Gaussian fitting. The Raman spectra of carbon materials typically show two modes: the G peak around 1580 - 1600 cm^{-1} corresponding to an ideal graphitic lattice vibration mode and the D peak around 1350 cm^{-1} corresponding to the defect lattice vibration mode.[28] In the spectral region between 1000-1800 cm^{-1} recent works reported three bands more associated with D band, indicating that these three extra peaks have to be also deconvoluted in order to obtained proper value of I_D/I_G ratio which is good parameter to estimate degree of defects in carbon network.[29] A peak centered at ~1620 cm^{-1} (D2) which can be observed as a shoulder of the G band is attributed to disorder-inducted phonon mode due to crystal defects.[29a] Other two bands, board peak between 1500 and 1550 cm^{-1} (D3) and smaller peak, as a shoulder of D peak, between 1150 and 1200 cm^{-1} (D4) are poorly understand.[29a] D3 band originates from amorphous carbon fraction since the intensity of D3 peak decrease with increase of crystallinity, while D4 peak could be attributed to disordered graphitic lattice provided by sp^2-sp^3 bonds at the edges of carbon network.[29,30] It is evident that spectra of all four carbon materials prepared within this study show beside two characteristic D and G bands also show D2, D3 and D4 bands. The ratios of I_D/I_G were found to be 1.9, 2.2, 2.3 and 2.5 for HTC+IL, ITC, HTC and Carb–IL, respectively. These large I_D/I_G ratios indicated the presence of a carbon structure with a number of defects. Higher I_D/I_G ratio for Carb–IL compared to other materials indicates more defects, which could be caused by the double doping of this material with nitrogen and sulphur atoms.[5d] Namely, it has been previously reported that introduction of heteroatoms in the carbon structure develops defect sites and increment of the I_D/I_G value in the Raman spectroscopy results.[14,31]

2.3 Study of oxygen reduction reaction

Cyclic voltammetry, as the first step of investigation of the prepared materials catalytic activity for the ORR, was performed in N_2- and O_2-saturated 0.1 M KOH solution. As can be seen in Figure 4, control CVs for all materials recorded in electrolyte saturated with N_2 showed no redox peaks. On the other hand, single cathodic peak was observed in O_2-saturated electrolyte for all four materials; a clear peak for Carb-IL and HTC and less pronounced peak for ITC and HTC+IL. This cathodic peak was observed at 0.33, 0.30 and 0.44 V for HTC, HTC+IL and ITC, respectively. The peak potential at Carb–IL shifted positively to 0.6 V suggesting superior catalytic activity of carbonized ionic liquid for the ORR compared to other synthetized materials based on glucose as a precursor. Similar result with cathodic peak at ca. 0.6 V was obtained for ORR on S-doped graphene and Mn_3O_4/CNT nanocomposite.[6d,32] Oxygen reduction peak at Carb-IL was positively shifted compared to reduction peak observed at graphitic carbon nitride (0.48 V) and palladium-graphitic carbon nitridenanocomposite (0.54 V).[33]

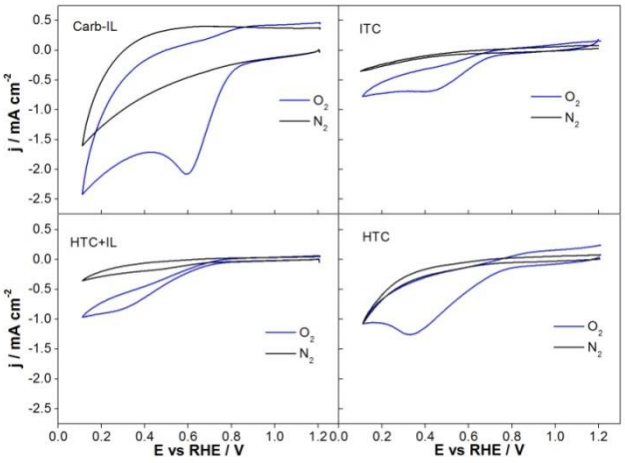

Figure 4. CV curves of Carb-IL, ITC, HTC+IL and HTC in N2- and O2-saturated 0.1 M KOH electrolyte.

In order to examine the ORR on these catalysts in detail, linear sweep voltammetry with a rotating disk electrode at different rotating speeds from 200 to 2000 rpm was employed. For interpretation of LSV RDE data and determination of number of electrons (n) used per O_2 molecule, the Koutecky–Levich (K–L) equation (Eq. 1) was used:

$$\frac{1}{j} = \frac{1}{j_k} + \frac{1}{j_d} = \frac{1}{j_k} + \frac{1}{0{,}62nFD_o^{2/3}\nu^{-1/6}C_o\omega^{1/2}} \quad (1)$$

where j, j_K and j_d represent the measured, kinetic and diffusion-limited current density, respectively, F is the Faraday constant (96485 C mol^{-1}), D_o is the diffusion coefficient of oxygen (1.9 × 10^{-5} cm^2 s^{-1}), v is the kinematic viscosity of electrolyte (0.01 cm^2 s^{-1}), C_o is the oxygen solubility (1.21×10^{-6}mol cm^{-3}) and ω is the electrode rotation rate.[6c] The number of electrons used per O_2 molecule can be calculated from the slope of Koutecky-Levich plots (j^{-1} *vs.* $\omega^{-1/2}$), constructed from the LSV diagrams recorded at different rotation rates. The results (Figure 5) show that ORR in the case of Carb–IL proceeds through direct four-electron pathway described by Eq. 2

$$O_2 + H_2O + 4e^- \rightarrow 4OH^- \quad (2)$$

Namely, Carb–IL gave similar n values (n = 4) within the whole investigated potential range from 0.5 to 0.2 V, while n value increased from 3 to 4 for HTC, from 2.2 to 2.78 for HTC+IL, and from 2.2 to 3.0 for ITC as the potential moved to lower values. The number of electrons transferred during ORR at HTC+IL and ITC corresponds to a dominant two-step two-electron pathway (Eq. 3 and 4).

$$O_2 + H_2O + 2e^- \rightarrow HO_2^- + OH^- \quad (3)$$

$$HO_2^- + H_2O + 2e^- \rightarrow 3OH^- \quad (4)$$

Number of electrons obtained for HTC suggests co-existence of two- and four-electron ORR pathway at this material.[34] Electrocatalysts efficiency for the ORR, i.e., the amount of HO_2^- generated is, to a great extent, governed by structure and thickness of the active layer. Thus, ORR efficiency differs for electrocatalyst with smooth surface and electrocatalyst with high-area active layer. It also differs if there is a barrier for the back–diffusion of the reaction intermediates. Namely, formed adsorbed HO_2^- can be directly reduced to H_2O. Conversely, adsorbed HO_2^- can desorb, diffuse into the diffusion layer and then either re-adsorb and reduce to H_2O, or diffuse into the electrolyte. The residence time of the intermediate species in the active layers of high surface-area substrates used in this study, is expected to be long enough to lead to further reduction of formed intermediates.[35]

For further comparison of the catalytic performance of prepared materials, kinetic current density (j_K) was calculated from the intercept of Koutecky-Levich plots constructed for potential of 0.2 V. The values of j_K were determined to be 5.5, 2.91, 2.45 and 0.9 mA cm^{-2} for Carb-IL, HTC, ITC and HTC+IL, respectively. These values confirmed that catalytic activity of Carb-IL is higher compared to that of other three materials. Furthermore, the j_K value at Carb-IL is higher than j_K values for Pt/C catalyst (5.1 mA cm^{-2}), sulphur-doped graphene prepared at 600°C (3.5 mA cm^{-2}), nitrogen- and sulphur-doped 3D graphene framework (3.9 mA cm^{-2}) and it is comparable with value for sulphur-doped graphene obtained at 900°C (5.3 mA cm^{-2}).[36] Furthermore, j_K value of Carb-IL is almost two time higher than value for non-doped carbon nanotubes and graphene (2.65 and 2.63 mA cm^{-2}).[37]

LSV curves at 1600 rpm reveal that Carb-IL also has higher diffusion limited current density (j_d) compared to the other three materials. Values of j_d for all materials decrease as the rotation rate decreases since diffusion distance of oxygen-saturated electrolyte is shortened at high speed.[38] Similarly to other carbon electrocatalysts doped with heteroatom or with transition metal, the polarization curves of four carbon materials studied herein do not show well-defined diffusion limiting current plateau at any rotation rate.[39] With increase of rotation rate, the plateau is more inclined, indicating that a complete diffusion control is not established, possibly due to less uniform distribution of the active sites on the electrocatalysts.[39a,40] Contrary to kinetic current density, j_d value of Carb-IL (2.9 mA cm^{-2}) is lower compared to the standard value for Pt/C catalyst (5.2 mA cm^{-2}), nitrogen and sulphur-codoped 3D reduced graphene oxide (5.23 mA cm^{-2}), sulphur-doped graphene (5 mA cm^{-2}), nitrogen-doped carbon nanosheets (5.78 mA cm^{-2}) and carbon nanoshell (5.1 mA cm^{-2}) at 0.2 V vs. RHE and 1600 rpm.[38,41] Current density values are influenced by the specific surface area of a material, as well as by the choice of binder. Pescarmona *et.al.* showed the negative influence of high Nafion loading on the overall current generation.[42] This contrast in j_d value of Carb-IL obtained in this paper compared to the mentioned materials could be explained by differences in the specific surface area. Carb-IL has lower value of specific surface area and consequently less active sites for electron transport and diffusion, contrary to the mentioned materials with higher specific surface area, resulting in lower value of j_d.[41b,41d] On the other hand, Carb-IL showed higher diffusion limited current density value compared to exfoliated graphene (~1.55 mA cm^{-2}), graphitic carbon nitride (~0.9 mA cm^{-2}), even carbon materials doped with noble metal such as palladium-graphitic carbon nitride nanocomposite (~1.6 mA cm^{-2}).[43,33]

The onset potentials for ORR were observed to be 0.84, 0.80, 0.79 and 0.89 V for HTC, HTC+IL, ITC and Carb–IL, respectively, similar to ORR onset potential values obtained from CV measurements. The ORR onset potential value at Carb-IL is comparable with the onset potential value at commercial Pt/C catalyst (0.93 V) and similar to onset potential values reported for other carbon-based materials such as sulphur- and nitrogen-dual doped mesoporous graphene (0.9 V), sulphur- and nitrogen-doped carbon aerogels (0.8 V), undoped and nitrogen-doped carbon nanotubes (0.8 V and 0.86 V, respectively).[7a,9a,44] It is also worth mentioning that ORR onset potential at Carb-IL is comparable or positive compared to onset potential values observed at carbon materials with noble metals such as palladium-graphitic carbon nitridenanocomposite (0.9 V), Ag-MWCNT (0.8 V), Au-graphene (0.71 V) and metals such as cobalt-nitrogen doped carbon (0.86 V) and cobalt-nitrogen doped reduced graphene oxide (0.9 V).[33,45] ORR activity of easily prepared Carb-IL is better or similar compare to series of nanocomposite Co_3O_4-$MnCo_2O_4$/N-doped reduced graphene oxide electrocatalysts.[34] Carbon materials prepared by carbonization of other ILs showed similar properties in terms of the ORR onset potential and mechanism. For example, ORR onset potential of ~0.9 V and ca. 4 electrons transferred were observed for carbons prepared using 1-butyl-1-methyl-pyrrolidinium bis((trifluoromethyl)sulfonyl)imide with eutectic salt

as template and 1-ethyl-3-methylimidazolimu dicyanamide using opal silica colloidal crystals as a hard template.[46] The herein proposed synthesis procedure is simpler compared to three latter methods, enabling preparation of Carb–IL material in one step route, without any template or additional substances, which is suitable for large scale production of electrocatalyst.

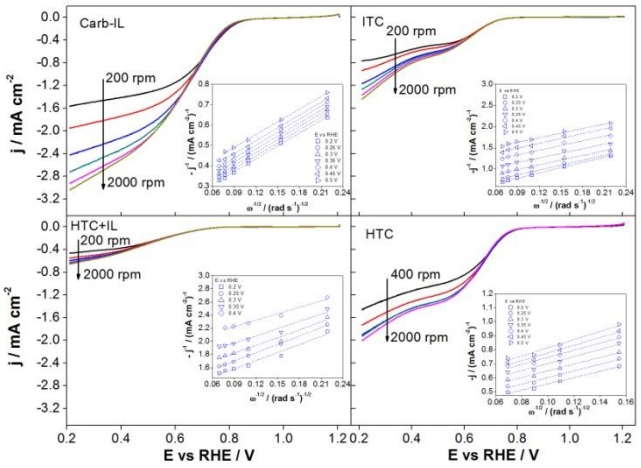

Figure 5. LSV curves and corresponding Koutecky-Levich plots of Carb-IL, ITC, HTC+IL and HTC.

Tafel analysis was next performed, with Figure 6 showing the mass-transport corrected Tafel plots for ORR on four electrocatalysts, obtained from the LSV curves with electrode rotation speed of 1600 rpm. The measured current densities were corrected for mass-transport to kinetic current densities (j_k) using Eq. 5:

$$j_k = \frac{j \cdot j_d}{(j_d - j)} \qquad (5)$$

where $j_d/(j_d - j)$ is the mass transfer correction factor. As can be seen in Figure 6, two Tafel regions (depending on the potential) could be observed for HTC (Tafel slope of 85.2 mV dec^{-1} and 99.5 mV dec^{-1}) and HTC+IL (Tafel slope of 114.6 mV dec^{-1} and 198.0 mV dec^{-1}). Contrary, a single Tafel slope was obtained for Carb-IL (104.4 mV dec^{-1}) and ITC (92.6 mV dec^{-1}). Single Tafel slope, with higher value compared to values obtained for Carb-IL and ITC, was also observed for Pt_3Ni (125 mV dec^{-1}) and Pt_3Co catalyst (118 mV dec^{-1}).[47] Also, higher single Tafel slope was reported for mesoporous carbon framework and mesoporous graphene framework (124 mV dec^{-1}) and for nitrogen-doped mesoporous graphene framework (115 mV dec^{-1}).[48]Other nitrogen codoped carbon materials showed lower Tafel slopes between 60-120 mV dec^{-1} such as: nitrogen-doped reduced graphene oxide (71.2 mV dec^{-1}), nitrogen-doped carbon nanotubes (65 and 113.8 mV dec^{-1}), ferrocene-based and iron(II) phthalocyanine-based nitrogen doped carbon nanotube (65 and 136 mV dec^{-1} and 87 and 171 mV dec^{-1}, respectively).[34,5a,49] Variation in coverage of adsorbed oxygen species could be described by Tafel slope and high values of obtained Tafel slopes in the range from 85.2 mV dec^{-1} to 198.0 mV dec^{-1} could indicate inefficient coverage of the adsorbed intermediates.[50] Still, it should be noted that Tafel slopes of HTC, ITC and Carb-IL fall in the range between 60 mV dec^{-1} and 120 mV dec^{-1}, values reported for Pt-based electrocatalysts.

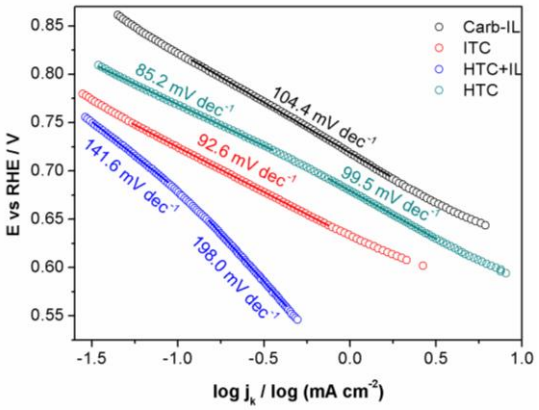

Figure 6. Tafel plots of four carbon materials obtained from the LSV curves shown in Figure 5.

Electrochemical impedance measurements were used to investigate the changes of interfacial electron – transfer properties. Semicircle diameter of Nyquist diagram (Figure 7 left) can be used to describe the charge transfer resistance at the electrode surface. The value of charge transfer resistance for HTC, ITC and HTC+IL was 619.2, 53.0 and 29.0 Ω, respectively. Compared to other materials, Carb–IL showed the smallest value of charge transfer resistance (27.7 Ω), indicating that Carb–IL can accelerate electron transfer leading to higher catalytic performance for the ORR.[37] According to the Bode plots (Figure 7 right), Carb-IL has the highest value of phase angle of ca. -60° at low frequencies which is less than the -90° expected for ideal capacitors. Still, Carb-IL is better capacitor compared to the other three material, as evident from the CVs shown in Figure 4 as well.[51]

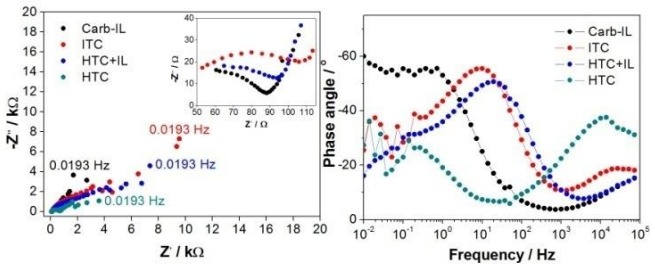

Figure 7. Direct comparison of Nyquist (left) and Bode (right) plots of Carb-IL, ITC, HTC+IL and HTC.

The more positive cathodic peak and onset potential, direct four – electron pathway and the smallest value of charge transfer resistance, indicate a strong improvement of the O_2 reduction kinetics at the Carb–IL electrode. These properties of Carb–IL could be attributed to the double doping of this material with sulphur and nitrogen. Carbon, sulphur and nitrogen atoms have different electronegativity (2.55; 2.58 and 3.04; respectively).[6d] The higher electronegativity of nitrogen atoms compared to

carbon atoms induces the positive charge density on the adjacent carbon atoms which is favourable for the ORR.[2,6d] Electronegativity of sulphur and carbon are similar, therefore, the charge transfers between them are negligible.[7a] On the other hand, double doping of carbons with sulphur and nitrogen atoms leads to increase of spin density indicating higher ORR catalytic performance.[7a] The sulphur atom has the largest atomic radius (100 pm) compared to nitrogen and carbon atoms (65 and 70 pm) and therefore sulphur atoms can induce larger defects in carbon structure compared to nitrogen-doped carbons, thus facilitating charge localization and chemisorption of oxygen.[9a] Also, nitrogen and sulphur functionalities in Carb-IL composition give rise to improved activity for the ORR. Some authors claim that the pyridinic-N tends to be the most active nitrogen functional group for ORR since formation of pyridinic-N is observed on the edge of graphite plane and its lone electrons pair acts as active site for the ORR.[5a,29d,52] On the other side, Luo *et al.* observed two-step two-electron ORR pathway on carbon containing only pyridinic-N; this result suggests that pyridinic-N cannot be the only responsible for enhancement of the ORR kinetics.[53] Herein, the amount of quaternary graphitic nitrogen is almost double compared to pyridinic nitrogen, indicating that graphitic nitrogen plays dominant role in enhancing the overall ORR activity of N-doped carbon materials; this is in agreement with results reported in the literature.[54] It is also necessary to take into account sulphur functional groups present in Carb-IL. Electrocatalytic activity for ORR is also enhanced with thiophene-like group, that accounts for the highest amount of the total sulphur content and acts as an active site for the increased ORR activity.[55] All these synergistic effects of double doping of carbon material with nitrogen and sulphur atoms and functionalities (quaternary graphitic nitrogen and thiophene-S) lead to enhanced electrocatalytic activity for ORR.

Other three materials also showed electrocatalytical activity for ORR, but significantly lower compared to Carb-IL. Since HTC, HTC+IL and ITC are non-doped, their activity originates from oxygen content and oxygen functionalities, which can promote oxygen reduction.[56] Beside oxygen functionalities and oxygen content, high specific surface area of HTC has contribution to oxygen reduction activity of this electrocatalyst.[5c]

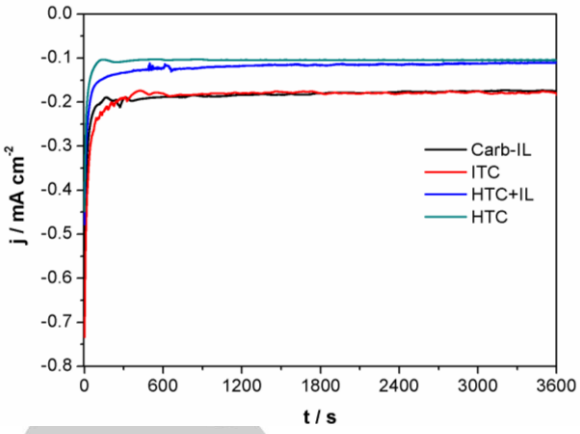

Figure 8.CA responses of HTC, HTC-IL, ITC and Carb-IL in O_2-saturated 0.1 M KOH at 0.5 V vs. RHE during 3600 s without rotation.

The stability of electrode material's activity for the ORR is an important property of fuel cells and it was herein examined by chronoamperometric measurements at potential of 0.5 V for 3600 s (Figure 8). After 500 s, all materials showed long-term stability, contrary to Pt/C electrode which was reported to show gradual current loss.[6d] The CA responses showed that Carb-IL and ITC have similar current decay during 3600 s. Current density reached constant values close to 0.2 mA cm^{-2} for Carb-IL and ITC and 0.1 mA cm^{-2} for HTC+IL and HTC.

Due to high electrocatalytic activity of Carb-IL for the ORR and possibility of its potential application in fuel cells, the selectivity of the Carb-IL catalyst towards ORR was further investigated. Carb-IL was examined in conditions typical for direct methanol fuel cell (DMFC), direct ethanol fuel cell (DEFC) and direct borohydride fuel cells (DBFC). Namely, methanol, ethanol and sodium borohydride were added to 0.1 M KOH, simulating their crossover from anodic to cathodic compartment, a general problem in practical fuel cells, in order to examine their influence on the ORR kinetics. As shown in Figure 9, the original cathodic current of Carb-IL remained nearly unchanged after addition of methanol, ethanol and sodium borohydride in the electrolyte solution. Contrary, Pt/C catalysts were reported to show sharp increase of current density upon addition of methanol, with this significant change in original current density affecting the performance of fuel cells.[57] These results imply that Carb-IL catalyst exhibits high selectivity for ORR and potential application as cathode material in DMFCs, DEFCs and DBFCs.

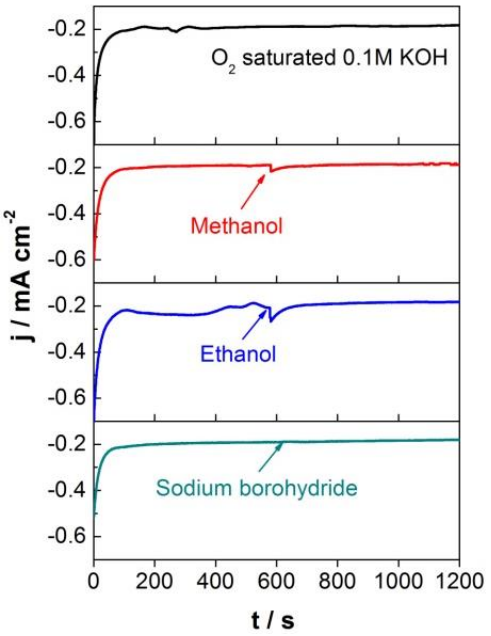

Figure 9. CA responses of Carb-IL in O_2-saturated 0.1 M KOH at 0.5 V vs. RHE without rotation, with addition of 3 M methanol, 3 M ethanol and 5 mg of sodium borohydride around 600ths.

Carbon material obtained by simple direct carbonization of ionic liquid clearly has attractive features for application as electrocatalyst for oxygen reduction reaction in alkaline fuel cells. Beside the simplicity of proposed direct carbonization of IL,

another advantage is low cost of Carb-IL compare to cost of Pt/C catalyst. The cost of Carb-IL catalyst, prepared by direct carbonization of [bmim][$MeSO_3$], for a 1 m^2 cathode is estimated to be around $100, significantly cheaper than Pt/C (around $2700). Still, there are some issues/imperfections related to synthesis procedure and the material propreties that could be improved. Probably the most significant is to obtain higher yield of carbon and higher surface area in order to reduce the cost of catalyst and to increase diffusion limited current density. Both objectives can be achieved by optimization of carbonization method.

3. Conclusions

Four carbon materials were synthesized using different precursors and procedures. SEM and N_2-sorption analysis revealed quite different morphology of the prepared samples. XPS analysis showed presence of nitrogen and sulphur only in Carb-IL, suggesting novel simple method of synthesis of double-doped carbon materials using ionic liquids as precursors. All four materials exhibited activity for the ORR in alkaline media. The RDE measurement showed ORR onset potentials in the 0.80 – 0.89 V region with Carb-IL showing the most positive onset potential among the four tested materials. The number of electrons exchanged during ORR was found to be ca. 4 for Carb-IL, between 3 and 4 for HTC and between 2 and 3 for HTC+IL and ITC, with higher current densities recorded at the two formers. Tafel slope values ranged from 85.2 mV dec^{-1} to 198.0 mV dec^{-1}. The lowest value of charge transfer resistance was determined for Carb-IL. Carb-IL was also studied for potential application as cathode materials in DMFCs, DEFCs and DBFCs, so the activity for ORR was examined in the presence of methanol, ethanol and borohydride in the supporting electrolyte. High activity for the ORR and stability in alkaline media, as well as its good methanol, ethanol and borohydride tolerance, strongly suggest potential application of Carb-IL catalyst as cathode material in DMFCs, DEFCs and DBFCs.

Experimental Section

Synthesis of carbon materials and recovery of studied ionic liquid

In a typical hydrothermal synthesis of carbon material, 20 mL of 2 M D(+) glucose (Sigma-Aldrich) aqueous solution was prepared. For the hydrothermal carbonization of D(+) glucose in the presence of ionic liquid, 5 g of [bmim][$MeSO_3$] (IoLiTec) was added to 20 mL of 2 M D(+) glucose aqueous solution. Ionothermal carbonization was performed by dissolving 3.75 g of D(+) glucose in 10 g of [bmim][$MeSO_3$]. These mixtures were placed into Teflon lined stainless steel autoclaves, heated up to 200°C and maintained at this temperature for 24 h. Obtained materials, denoted as HTC@200, HTC+IL@200 and ITC@200 respectively, were washed with 20 mL of methanol and 50 mL of deionized water, filtered through filter paper and then dried at 80°C for 24 h. All materials were additionally thermally treated at 900°C for 1 h under N_2 atmosphere, with heating rate of 10°C min^{-1} and N_2 flow rate of 35 cm^3 min^{-1}. Finally, obtained materials were marked as HTC, HTC+IL and ITC, respectively. Direct carbonization of IL was performed under the same conditions as additional thermal treatment of materials and obtained carbon was marked as Carb–IL.

The melting temperature of [bmim][$MeSO_3$] was determined by means of the HLM method using AT-HLM prototype. 0.1 g of [bmim][$MeSO_3$] was placed into the plastic cell and used for analysis. After the ionothermal carbonization of glucose, the used [bmim][$MeSO_3$] was recovered from methanol fraction obtained after washing the synthesized material by evaporation of methanol using rotary evaporator. The recycled IL was filtered through porous membrane filter (pore diameter of 0.22 μm) in order to remove the impurities generated in the carbonization process. Recycled and pure IL was analysed with FT-IR and Raman spectroscopy. FT-IR spectra were recorded on Avatar 370 FTIR spectrometer (Thermo Nicolet) in the range of 4000–400 cm^{-1} at 64 scans per spectrum at 2 cm^{-1} resolution. For this analysis, samples were mixed with potassium bromide and compressed into pellets. Raman spectra were recorded on DXR Raman Microscope (Thermo Scientific).

Characterisation of carbon materials

The morphology of the prepared carbon materials was examined by scanning electron microscopy (SEM) using a JEOL JSM 7001F microscope. The specific surface area of samples (S_{BET}) was calculated by applying the Brunauer–Emmett–Teller equation from the linear part of the adsorption isotherm obtained by nitrogen adsorption at -196 °C using a Sorptomatic 1990 Thermo Finnigan device. Prior to adsorption, the samples were first degassed for 2 h at room temperature under vacuum and then at 200 °C for 24 h at the same residual pressure. The XPS analysis was performed using a Kratos AXIS Ultra HAS spectrometer, with VISION software for data acquisition and CASAXPS software for data analysis. The analysis was carried out with a monochromatic Al Kα X-ray source (1486.7 eV) operating at 15kV (90 W) in FAT (Fixed Analyser Transmission) mode, with a pass energy of 40 eV for regions of interest and 80 eV for survey. The powder samples were adhered to carbon tape for analysis; thus, detection of Si in all analysis indicates the possibility of the carbon tape exposure. Again, Raman spectra were recorded on DXR Raman Microscope (Thermo Scientific) using 5 mW of laser power.

Electrode preparation and electrochemical measurements

To prepare the working electrodes, 5 mg of each carbon material was dispersed in 1 mL of deionized water and 0.03 mL of 5% Nafion (Sigma-Aldrich). The mixture was sonicated for 30 min at room temperature to obtain homogenous catalytic ink. 10 μL of the ink was dropped on the glassy carbon electrode (5 mm diameter) previously polished and washed with deionized water and ethanol and, finally, the modified electrode was dried.

All electrochemical measurements were performed at the Gamry PCI4/750 potentiostat/galvanostat using one-compartment cell with three-electrode setup. The electrochemical cell was composed of the modified glassy carbon as working electrode, platinum counter electrode, saturated calomel electrode (SCE) as the reference electrode and 25 mL of 0.1 M KOH (Sigma-Aldrich) aqueous solution as the electrolyte. All potentials in the paper are given relative to the reversible hydrogen electrode (RHE), converted using the formula: $E_{RHE} = E_{SCE} + 0.242 + 0.059 \cdot pH$. Prior to each measurement, the electrolyte was saturated with high purity N_2 or O_2 gas for 20 min. Cyclic voltammetry (CV) tests were performed from 1.2 V to 0.1 V at sweep rate of 100 mVs^{-1}. The linear sweep voltammetry (LSV) experiments were conducted with the modified glassy carbon rotating disk electrode (RDE) from 1.2 V to 0.2 V at scan rate of 5 mVs^{-1} and various rotating speeds from 200 to 2000 rpm. RDE currents recorded in O_2-saturated electrolyte were corrected for background currents by subtracting the currents recorded in the N_2-saturated electrolyte. Electrochemical impedance spectroscopy (EIS)

was run at potential of oxygen reduction within frequency interval ranging from 0.01 Hz to 100 kHz, keeping always the same geometry of electrodes. Chronoamperometry (CA) experiments with all materials registered the current change with time while keeping the potential at constant value of 0.5 V for 3600 s. All presented current densities were calculated using the electrode geometric area (0.19625 cm^2).

Acknowledgements

The Ministry of Education, Science and Technological Development of Republic of Serbia is acknowledged for support within project Nos. III45006, III45014 and III45001. Associate professor Igor Pašti (FPC, UB) is acknowledge for the help with the discussion of the results. The Associate Laboratory LSRE-LCM (Project POCI-01-0145-FEDER-006984) was funded by ERDF through COMPETE2020 – Programa Operacional Competitividade e Internacionalização (POCI) – and by national funds through FCT - Fundação para a Ciência e a Tecnologia. RPR also acknowledges FCT for grant SFRH/BD/95411/2013. Dr. Carlos Sá (CEMUP) is acknowledged for assistance with XPS analyses. Financial support of the Ministry of Education, Sports, and Youth of the Czech Republic under grant No. COST LD14090 and the COST Action CM1206 EXILis acknowledged by M. Bendova. Dr. François Quirion is gratefully acknowledged for providing the team at ICPF with the prototype AT-HLM for carrying out the HLM analyses.

Keywords: ionic liquids • porous carbon materials •ionothermal carbonization • oxygen reduction reaction • fuel cells

[1] a) B. Šljukić, C. E. Banks, R. G. Compton, *J. Iran. Chem. Soc.* **2005**, *2*, 1–25; b) X. Ren, S. S. Zhang, D. T. Tran, J. Read, *J. Mater. Chem.* **2011**, *21*, 10118–10125.

[2] L. Zhang, Z. Xia, *J. Phys. Chem. C* **2011**, *115*, 11170–11176.

[3] a) T. J. Schmidt, U. A. Paulus, H. A. Gasteiger, R. J. Behm, *J. Electroanal. Chem.* **2001**, *508*, 41–47; b) M. Neergat, A. K. Shukla, K. S. Gandhi, *J. Appl. Electrochem* .**2001**, *31*, 373–378; c) L. Zhang, J. Zhang, D. P. Wilkinson, H. Wang, *J. Power Sources* **2006**, *156*, 171–182.

[4] N. Daems, X. Sheng, I. F. J. Vankelecom, P. P. Pescarmona, *J. Mater. Chem. A* **2014**, *2*, 4085–4110.

[5] a) Z. Chen, D. Higgins, H. Tao, R. S. Hsu, Z. Chen, *J. Phys. Chem. C* **2009**, *113*, 21008–21013; b) D. Geng, Y. Chen, Y. Chen, Y. Li, R. Li, X. Sun, S. Ye, S. Knights, *Energy Environ. Sci.* **2011**, *4*, 760–764; c) S. Chen, J. Bi, Y. Zhao, L. Yang, C. Zhang, Y. Ma, Q. Wu, X. Wang, Z. Hu, *Adv. Mater.* **2012**, *24*, 5593–5597; d) W. Ouyang, D. Zeng, X. Yu, F. Xie, W. Zhang, J. Chen, J. Yan, F. Xie, L. Wang, H. Meng, et al., *Int. J. Hydrogen Energy* **2014**, *39*, 15996–16005.

[6] a) L. Yang, S. Jiang, Y. Zhao, L. Zhu, S. Chen, X. Wang, Q. Wu, J. Ma, Y. Ma, Z. Hu, *Angew. Chemie* **2011**, *123*, 7270–7273; b) R. Li, Z. Wei, X. Gou, W. Xu, *RSC Adv.* **2013**, *3*, 9978–9984; c) J. Wu, Z. Yang, X. Li, Q. Sun, C. Jin, P. Strasser, R. Yang, *J. Mater. Chem. A***2013**, *1*, 9889-9896; d) Z. Yang, Z. Yao, G. Li, G. Fang, H. Nie, Z. Liu, X. Zhou, X. Chen, S. Huang, *ACS Nano* **2012**, *6*, 205–211; e) C. H. Choi, M. W. Chung, Y. J. Jun, S. I. Woo, *RSC Adv.* **2013**, *3*, 12417-12422; f) Z. Yao, H. Nie, Z. Yang, X. Zhou, Z. Liu, S. Huang, *Chem. Commun.* **2012**, *48*, 1027–1029.

[7] a) J. Liang, Y. Jiao, M. Jaroniec, S. Z. Qiao, *Angew. Chemie Int. Ed.* **2012**, *51*, 11496–11500; b) C. H. Choi, S. H. Park, S. I. Woo, *ACS Nano* **2012**, *6*, 7084–7091; c) C. H. Choi, S. H. Park, S. I. Woo, *J. Mater. Chem.* **2012**, *22*, 12107–12115.

[8] M.-M. Titirici, M. Antonietti, *Chem. Soc. Rev.***2010**, *39*, 103–116.

[9] a) S.-A. Wohlgemuth, R. J. White, M.-G. Willinger, M.-M. Titirici, M. Antonietti, *Green Chem.* **2012**, *14*, 1515–1523; b) S.-A. Wohlgemuth, T.-P. Fellinger, P. Jäker, M. Antonietti, *J. Mater. Chem. A***2013**, *1*, 4002-4009; c) A. Kalijadis, J. Đorđević, T. Trtić-Petrović, M. Vukčević, M. Popović, V. Maksimović, Z. Rakočević, Z. Laušević, *Carbon N. Y.***2015**, *95*, 42–50; d) G. Ćirić-Marjanović, I. Pašti, N. Gavrilov, A. Janošević, S. Mentus, *Chem. Pap.***2013**, *67*, 781–813.

[10] Z.-L. Xie, D. S. Su, *Eur. J. Inorg. Chem.* **2015**, *2015*, 1137–1147.

[11] J. S. Lee, R. T. Mayes, H. Luo, S. Dai, *Carbon N. Y.***2010**, *48*, 3364–3368.

[12] a) P. Zhang, Y. Gong, Z. Wei, J. Wang, Z. Zhang, H. Li, S. Dai, Y. Wang, *ACS Appl. Mater. Interfaces***2014**, *6*, 12515–12522; b) M.-M. Titirici, A. Thomas, M. Antonietti, *Adv. Funct. Mater.***2007**, *17*, 1010–1018.

[13] Z.-L. Xie, R. J. White, J. Weber, A. Taubert, M. M. Titirici, *J. Mater. Chem.***2011**, *21*, 7434–7442.

[14] X.-X. Lin, B. Tan, L. Peng, Z.-F. Wu, Z.-L. Xie, *J. Mater. Chem. A***2016**, *4*, 4497–4505.

[15] a) S. Zhang, K. Dokko, M. Watanabe, *Chem. Mater.***2014**, *26*, 2915–2926; b) J. S. Lee, X. Wang, H. Luo, S. Dai, *Adv. Mater.***2010**, *22*, 1004–1007.

[16] F. Quirion, D. Lambert, G. Perron, *Can. J. Chem.***1992**, *70*, 2745–2750.

[17] G. Perron, A. Hardy, J.-C. Justice, J. E. Desnoyers, *J. Solution Chem.***1993**, *22*, 1159–1178.

[18] P. Kovanic, M. B. Humber, The economics of information-mathematical gnostics for data analysis, book 717 pp [on-line], available only online at http://www.math-gnostics.eu/books.

[19] S. Kudo, Z. Zhou, K. Yamasaki, K. Norinaga, J. Hayashi, *Catalysts***2013**, *3*, 757–773.

[20] M.-M. Titirici, M. Antonietti, N. Baccile, *Green Chem.***2008**, *10*, 1204–1212.

[21] P. Zhang, Y. Gong, Z. Wei, J. Wang, Z. Zhang, H. Li, S. Dai, Y. Wang, *ACS Appl. Mater. Interfaces***2014**, *6*, 12515–12522.

[22] J. S. Lee, X. Wang, H. Luo, G. A. Baker, S. Dai, *J. Am. Chem. Soc.***2009**, *131*, 4596–4597.

[23] J. P. Paraknowitsch, A. Thomas, *Macromol. Chem. Phys.***2012**, *213*, 1132–1145.

[24] a) J. P. Paraknowitsch, A. Thomas, M. Antonietti, *J. Mater. Chem.***2010**, *20*, 6746–6758; b) T. J. Wooster, K. M. Johanson, K. J. Fraser, D. R. MacFarlane, J. L. Scott, *Green Chem.***2006**, *8*, 691–696.

[25] M. Enterría, J. L. Figueiredo, *Carbon* **2016**, *108*, 79–102.

[26] W. Kiciński, M. Szala, M. Bystrzejewski, *Carbon* **2014**, *68*, 1–32.

[27] a) M. Favaro, F. Carraro, M. Cattelan, L. Colazzo, C. Durante, M. Sambi, A. Gennaro, S. Agnoli, G. Granozzi, *J. Mater. Chem. A***2015**, *3*, 14334–14347; b) D. Sun, J. Yang, X. Yan, *Chem. Commun.***2015**, *51*, 2134–2137.

[28] A. C. Ferrari, J. Robertson, *Phys. Rev. B***2000**, *61*, 14095–14107.

[29] a) S. Claramunt, A. Varea, D. López-Díaz, M. M. Velázquez, A. Cornet, A. Cirera, J. Phys. Chem. C **2015**, 119, 10123–10129; b) A. Sadezky, H. Muckenhuber, H. Grothe, R. Niessner, U. Pöschl, Carbon **2005**, 43, 1731–1742; c) S. Vollebregt, R. Ishihara, F. D. Tichelaar, Y. Hou, C. I. M. Beenakker, Carbon **2012**, 50, 3542–3554; d) S. Maldonado, S. Morin, K. J. Stevenson, *Carbon* **2006**, *44*, 1429–1437.

[30] A. Cuesta, P. Dhamelincourt, J. Laureyns, A. Martínez-Alonso, J. M. D. Tascón, Carbon **1994**, 32, 1523–1532.

[31] Z. R. Ismagilov, A. E. Shalagina, O. Y. Podyacheva, A. V. Ischenko, L. S. Kibis, A. I. Boronin, Y. A. Chesalov, D. I. Kochubey, A. I. Romanenko, O. B. Anikeeva, et al., *Carbon* **2009**, *47*, 1922–1929.

[32] D. Huang, B. Zhang, S. Li, M. Wang, Y. Shen, *ChemElectroChem***2014**, *1*, 1531–1536.

[33] S. K. Konda, M. Amiri, A. Chen, *J. Phys. Chem. C* **2016**, *120*, 14467–14473.

[34] X. He, F. Yin, S. Yuan, N. Liu, X. Huang, *ChemElectroChem* **2016**, *3*, 1107–1115.

[35] B. Šljukić, M. Martins, E. Kayhan, A. Balčiūnaitė, T. Şener, C. A. C. Sequeira, D. M. F. Santos, *J. Electroanal. Chem.* **2017**, *797*, 23–30.

[36] a) S. Yang, L. Zhi, K. Tang, X. Feng, J. Maier, K. Müllen, *Adv. Funct. Mater.* **2012**, *22*, 3634–3640; b) Y. Su, Y. Zhang, X. Zhuang, S. Li, D. Wu, F. Zhang, X. Feng, *Carbon* **2013**, 62, 296–301.

[37] Z. Jin, H. Nie, Z. Yang, J. Zhang, Z. Liu, X. Xu, S. Huang, *Nanoscale* **2012**, *4*, 6455–6460

[38] L. Huo, B. Liu, G. Zhang, R. Si, J. Liu, J. Zhang, *J. Mater. Chem. A* **2017**, 5, 4868–4878.

[39] a) W. Hu, N. Yoshida, Y. Hirota, S. Tanaka, N. Nishiyama, *Electrochem. commun*. **2017**, 75, 9–12; b) D. S. Yang, D. Bhattacharjya, S. Inamdar, J. Park, J. S. Yu, *J. Am. Chem. Soc.* **2012**, 134, 16127–16130; c) T. Palaniselvam, V. Kashyap, S. N. Bhange, J.-B. Baek, S. Kurungot, *Adv. Funct. Mater*. **2016**, 26, 2150–2162

[40] a) S. Ye, A. K. Vijh, *J. Solid State Electrochem*. **2005**, 9, 146–153; b) H.J. Zhang, Q.Z. Jiang, L. Sun, X. Yuan, Z.F. Ma, *Electrochim. Acta*

2010, 55, 1107–1112.

[41] a) Y. Li, J. Yang, J. Huang, Y. Zhou, K. Xu, N. Zhao, X. Cheng, *Carbon* **2017**, 122, 237–246; b) Y. Zhang, M. Chu, L. Yang, W. Deng, Y. Tan, M. Ma, Q. Xie, *Chem. Commun*. **2014**, 50, 6382-6385; c) W. Wei, H. Liang, K. Parvez, X. Zhuang, X. Feng, K. Müllen, *Angew. Chemie* **2014**, 126, 1596–1600; d) Y. Wang, A. Kong, X. Chen, Q. Lin, P. Feng, *ACS Catal*. **2015**, 5, 3887–3893

[42] N. Daems, T. Breugelmans, I.F. J. Vankelecom, P.P. Pescarmona, *ChemElectroChem* **2017**, doi:10.1002/celc.201700907

[43] B. J. Kim, D. U. Lee, J. Wu, D. Higgins, A. Yu, Z. Chen, *J. Phys. Chem. C* **2013**, 117, 26501–26508.

[44] N. Alexeyeva, E. Shulga, V. Kisand, I. Kink, K. Tammeveski, *J. Electroanal. Chem.***2010**, *648*, 169–175.

[45] a) Y. Cheng, W. Li, X. Fan, J. Liu, W. Xu, C. Yan, *Electrochim. Acta***2013**, *111*, 635–641; b) S.-S. Kim, Y.-R. Kim, T. D. Chung, B.-H. Sohn, *Adv. Funct. Mater.***2014**, *24*, 2764–2771; c) S. Lee, Y. W. Lee, D. H. Kwak, J. Y. Lee, S. B. Han, J. I. Sohn, K. W. Park, *J. Ind. Eng. Chem.***2016**, *43*, 170–176; d) T. Kottakkat, M. Bron, *ChemElectroChem***2014**, *1*, 2163–2171.

[46] a) Z. Cui, S. Wang, Y. Zhang, M. Cao, *J. Power Sources***2014**, *259*, 138–144; b) S. Zhang, H. M. Kwon, Z. Li, A. Ikoma, K. Dokko, M. Watanabe, *ChemElectroChem***2015**, *2*, 1080–1085.

[47] V. Stamenković, T. J. Schmidt, A. P. N. Ross, N. M. Marković, *J. Phys. Chem. B***2002**, *106*, 11970–11979.

[48] C. Zhang, B. Wang, X. Shen, J. Liu, X. Kong, S. S. C. Chuang, D. Yang, A. Dong, Z. Peng, *Nano Energy***2016**, *30*, 503–510.

[49] Z. Chen, D. Higgins, Z. Chen, *Electrochim. Acta* **2010**, 55, 4799–4804.

[50] S. M. Unni, V. M. Dhavale, V. K. Pillai, S. Kurungot, *J. Phys. Chem. C***2010**, *114*, 14654–14661.

[51] J. L. Qi, X. Wang, J. H. Lin, F. Zhang, J. C. Feng, W.-D. Fei, *J. Mater. Chem. A* **2015**, *3*, 12396–12403.

[52] a) Z. Chen, D. Higgins, Z. Chen, *Carbon* **2010**, *48*, 3057–3065; b) H. Li, W. Kang, L. Wang, Q. Yue, S. Xu, H. Wang, J. Liu, *Carbon* **2013**, *54*, 249–257.

[53] Z. Luo, S. Lim, Z. Tian, J. Shang, L. Lai, B. MacDonald, C. Fu, Z. Shen, T. Yu, J. Lin, *J. Mater. Chem.***2011**, *21*, 8038–8044.

[54] a) B. Zheng, J. Wang, F.-B. Wang, X.-H. Xia, *Electrochem. commun.***2013**, *28*, 24–26; b) H. Niwa, K. Horiba, Y. Harada, M. Oshima, T. Ikeda, K. Terakura, J. ichi Ozaki, S. Miyata, *J. Power Sources***2009**, *187*, 93–97.

[55] a) D.-H. Kwak, S.-B. Han, Y.-W. Lee, H.-S. Park, I.-A. Choi, K.-B. Ma, M.-C. Kim, S.-J. Kim, D.-H. Kim, J.-I. Sohn, et al., *Appl. Catal. B Environ.***2017**, *203*, 889–898; b) X. Qing, J. Shi, C. Ma, M. Fan, Z. Bai, Z. Chen, J. Qiao, J. Zhang, *J. Power Sources***2014**, *266*, 88–98; c) C. You, S. Liao, H. Li, S. Hou, H. Peng, X. Zeng, F. Liu, R. Zheng, Z. Fu, Y. Li, *Carbon N. Y.***2014**, *69*, 294–301.

[56] a) K. Matsubara, K. Waki, *Electrochem. Solid-State Lett.***2010**, *13*, F7-F9; b) D. Deng, L. Yu, X. Pan, S. Wang, X. Chen, P. Hu, L. Sun, X. Bao, *Chem. Commun.***2011**, *47*, 10016-10018.

[57] E. Bayram, G. Yilmaz, S. Mukerjee, *Appl. Catal. B Environ.***2016**, *192*, 26–34.

10.1002/celc.201701369

WILEY-VCH

Entry for the Table of Contents (Please choose one layout)

Layout 2:

ARTICLE

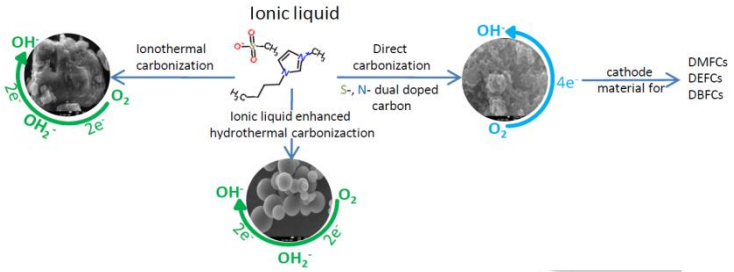

Carbon materials were synthetized using ionic liquid (IL) and tested as electrocatalysts for oxygen reduction reaction (ORR). Different morphology, structure, surface composition and ORR activity are reported. Carbon prepared by direct carbonisation of IL shows high ORR activity with 4e- exchanged.

*Nikola Zdolšek, Aleksandra Dimitrijević, Magdalena Bendova,Jugoslav Krstić,Raquel P. Rocha,José L. Figueiredo, Danica Bajuk-Bogdanović, Tatjana Trtić-Petrović and Biljana Šljukić**

Page No. – Page No.

Electrocatalytical activity of ionic liquid-derived porous carbon materials for oxygen reduction reaction